

THE MICROSTRUCTURE AND PROPERTIES OF MATERIALS AT THE FUSION LINE

Received - Primljeno: 2004-03-23

Accepted - Prihvaćeno: 2004-05-20

Original Scientific Paper - Izvorni znanstveni rad

In this paper, the formation of the HAZ that is caused by the thermal effects of welding is investigated from the theoretical and experimental points of view. Samples of the material found at the fusion line were prepared by simulating the thermal regimes that occur during welding. A number of CCT diagrams that are valid for the conditions during welding were designed, and the hardness and impact-toughness of the samples were measured. This information was then related to the results of metallographic examinations. The maximum temperature and the cooling rate of the applied thermal cycles were found to be decisive in terms of the properties of the HAZ.

Key words: *welding, heat-affected zone, thermal cycle, cooling rate, fusion line*

Mikrostruktura i svojstva materijala uz crtu taljenja. U ovom članku je sa teorijskog i eksperimentalnog motrišta istraživano ustrojstvo zone utjecaja topline (ZUT-a) koji je prouzrokovan termičkim utjecajima zavarivanja. Uzorci materijala, koji se nalazi uz crtu taljenja, bili su pripremljeni simulacijom termičkog postupka za vrijeme zavarivanja. Ustrojeno je više CCT dijagrama, koji važe za uvjete zavarivanja, a mjereni su takođe i tvrdoća te žilavost uzorka. Ti podaci su zatim uspoređeni sa rezultatima metalografskih ispitivanja. Obzirom na svojstva ZUT odlučujući su najviša temperatura primjenjenih termičkih ciklusa i brzina hlađenja.

Ključne riječi: *zavarivanje, zona utjecaja topline, termički ciklus, brzina hlađenja, crta taljenja*

INTRODUCTION

The heat required during fusion welding has an effect on the base metal (BM) close to the joint [1]. This affected region is referred to as the heat-affected zone (HAZ). During the heating process and the local fusing of the BM while the joint is being created, the temperature reaches a maximum, with the highest temperatures being found close to the zone of fusion. During cooling, however, similar temperatures occur across the whole joint.

Technical metals are polycrystalline materials, and their properties depend on their microstructures. During the processing of welded products, where joining is often the last step, the thermal cycle changes the microstructure wherever a critical temperature is exceeded. As a result, the final microstructure is a consequence of the chemical composition, the thermal treatment and the starting microstructure.

The aim of this article is to show that the microstructure and the properties of the HAZ are predictable if the parameters of the welding and the properties of the BM are taken into account. The thermal regime during weld-

ing can be simulated using a thermal-cycle simulator. In this article, the focus was on thick-plate welding with a high-strength low-alloy (HSLA) structural steel.

THE THERMAL TREATMENT OF MATERIAL DURING FUSION WELDING

During the process of seam, welding a moving heat-source is used to join the plates. In order to theoretically determine the temperature field the first and second laws of thermodynamics must be obeyed. If a point heat-source with a constant net power, P_{net} , moves in a straight line on a thick plate with a constant speed, v , peak temperature, T_p , at a distance R to the trajectory [2], then

$$T_p = T_0 + \frac{2P_{net}}{\pi \epsilon \rho c_v v} \cdot \frac{1}{R^2} \quad (1)$$

where T_0 is the starting temperature, and ρ and c_v are the density and thermal capacity of the material. Equation (1) represents the so-called three-dimensional cooling characteristic of thick-plate welding.

If $t \gg R/v$, the temperature, T , at point R decreases during cooling as

V. Gliha, Faculty of Mechanical Engineering University of Maribor, Maribor, Slovenia

$$T = \frac{Q_{net}}{2\pi\lambda t} \cdot e^{-\frac{R^2}{4Dt}} \quad (2)$$

where Q_{net} is the net heat input ($Q = P/v$), and D and λ are the thermal diffusivity and conductivity.

The cooling time $\Delta t_{8/5}$ is a suitable measure of the cooling rate in the case of carbon-steel welding [1]. It is the time taken for the material to cool from 800 to 500 °C, if the thickness, d , ensures three-dimensional cooling:

$$\Delta t_{8/5} = \frac{Q_{net}}{2\pi\lambda} \cdot \left(\frac{1}{500 - T_0} - \frac{1}{800 - T_0} \right);$$

$$d \geq \sqrt{\frac{Q_{net}}{2\rho c_v} \cdot \left(\frac{1}{500 - T_0} + \frac{1}{800 - T_0} \right)} \quad (3)$$

For typical workshop welding techniques, the conditions for three-dimensional cooling are fulfilled when the plate's thickness exceeds 20 to 30 mm.

The material properties in the above equations are temperature dependent. The average values in the temperature range where the austenite decomposes during cooling should be used in order to calculate appropriate values for $\Delta t_{8/5}$ and d [2, 3].

THE MATERIAL AND ITS PREPARATION

The chemical composition, the mechanical properties and the microstructure of the HSLA structural steel, which was delivered in the as-quenched-and-tempered state, are shown in Table 1. and Figure 1.

Table 1. **Chemical composition and mechanical properties of the BM**
 Tablica 1. **Kemijski sastav i mehanička svojstva osnovnog materijala**

Element	C	Si	Mn	P	S	Cr
mass / %	0,09	0,27	0,30	0,015	0,010	1,05
Element	Mo	Ni	V	Al	Ti	
mass / %	0,27	2,63	0,07	0,045	0,026	
R_p / MPa	R_m / MPa	A_5 / %	CVN / J	- 40	- 60	- 80 °C
713	764	17		170	155	120

Different sub-zones found at the fusion line (FL) were prepared on pieces of BM with sizes 11×11×55 mm. Two kinds of HAZ microstructure at the FL were analysed; they result from the influence of single and double thermal cycles. A metallographic examination was performed in order to determine the micro-constituents.

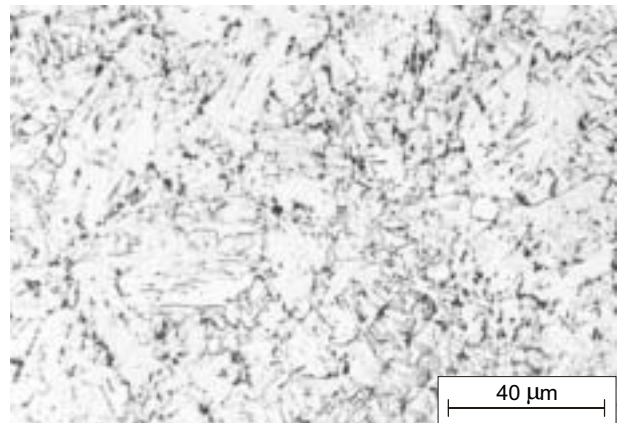


Figure 1. **Microstructure of the as-delivered steel consisting of tempered martensite and bainite**
 Slika 1. **Mikrostruktura čelika u isporučenom stanju sastoji se od martenzita i bainita**

A coarse-grained heat-affected zone (CGHAZ) is the result if the heat during welding significantly affects the material at the FL only once [4]. The BM is heated for a while close to its melting point, i.e. at least to $T_p = 1350$ °C, and then cooled in accordance with its thermo-mechanical properties and thickness (Equations (2) and (3)). The type of micro-constituents formed depends on the $\Delta t_{8/5}$ (Equation (3)). The characteristics of a CGHAZ are coarse grains, increased hardness and low toughness [5].

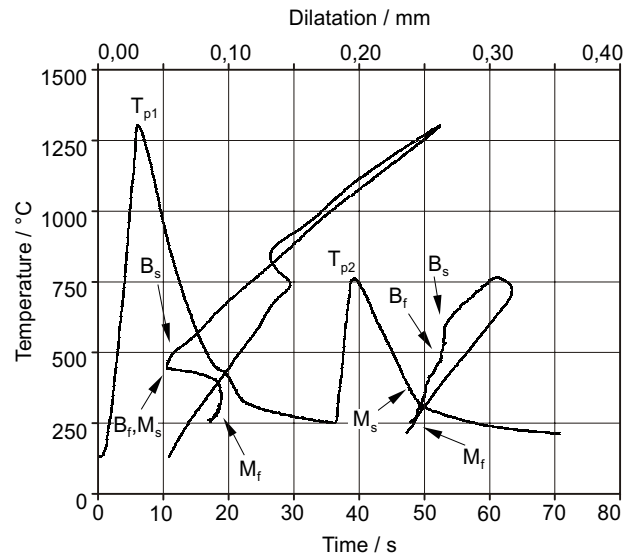


Figure 2. **Temperature course during the first ($T_{p1} \approx 1350$ °C) and the subsequent ($T_{p2} \approx 1350$ °C) thermal cycles at $\Delta t_{8/5} \approx 9$ s (1st cycle) and $\Delta t_{8/5} \approx 18$ s (2nd cycle). The dilatometry curves were recorded during the thermal cycles**

Slika 2. **Temperatura za vrijeme prvog ($T_{p1} \approx 1350$ °C) i sljedećeg ($T_{p2} \approx 1350$ °C) termičkog ciklusa kod $\Delta t_{8/5} \approx 9$ s (1. ciklus) i $\Delta t_{8/5} \approx 18$ s (2. ciklus). Zabilježene su dilatometrijske krivulje za vrijeme termičkog ciklusa**

Multi-pass welding is used when thicker plates need to be joined. The subsequent weld passes result in a short-term reheating of the initial coarse-grained microstructure at the FL. Depending on the T_p (Equation (1)) the CGHAZ can be re-transformed completely or partially. The result is either an over- or inter-critically reheated CGHAZ, i.e. OCCGHAZ ($T_{p2} > A_{c3}$) or ICCGHAZ ($A_{c1} < T_{p2} < A_{c3}$) [4]. The final microstructures and properties depend on the previous grain size, the T_p and the $\Delta t_{8/5}$.

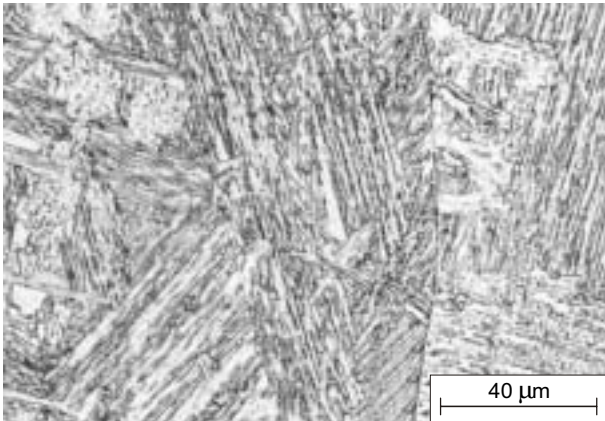


Figure 3. Microstructure of the simulated CGHAZ formed at $\Delta t_{8/5} \cong 25$ s, consisting of bainite and martensite.

Slika 3. Mikrostruktura simuliranog grubozrnatog ZUT formirana kod $\Delta t_{8/5} \cong 25$ s, sastoji se od bainita i martenzita

In order to prepare samples of material with microstructures that reflect a certain type of HAZ sub-zone, the same thermal regimes as those used during welding are required:

- in the case of the CGHAZ simulation the pieces of BM were heated at a rate of 200 K/s to $T_p \cong 1350$ °C. The

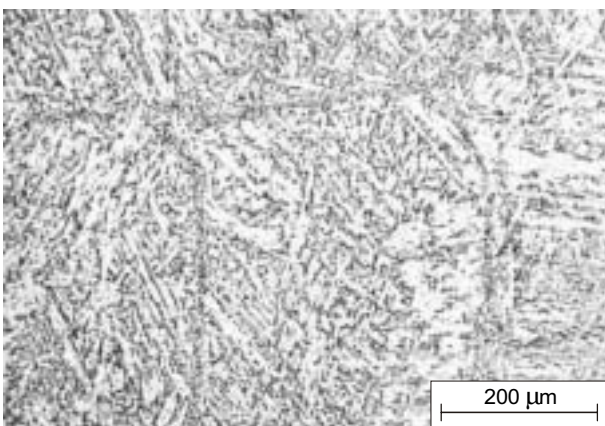


Figure 4. Microstructure of simulated ICCGHAZ formed at $\Delta t_{8/5} \cong 25$ s ($\Delta t_{5/3} \cong 50$ s), consisting of martensite and bainite

Slika 4. Mikrostruktura simuliranog interkritički zagrijanog grubozrnatog ZUT formirana kod $\Delta t_{8/5} \cong 25$ s ($\Delta t_{5/3} \cong 50$ s), sastoji se od martenzita i bainita

cooling rate was calculated according to Equation (2) so as to achieve the chosen $\Delta t_{8/5}$. Such a thermal cycle is shown in Figure 2. (1st cycle with T_p designated as T_{p1}). The microstructure of the CGHAZ formed at $\Delta t_{8/5} \cong 25$ s is shown in Figure 3,

- in the case of the OCCGHAZ and ICCGHAZ simulations the pieces of BM were first heated at a rate of 200 K/s to $T_{p1} \cong 1350$ °C, as in the case of the CGHAZ simulation. After cooling to approximately 200 °C, in accordance with Equation (2) (1st cycle in Figure 2.), the pieces were heated at a rate of 100 K/s to $T_{p2} \cong 960$ °C (OCCGHAZ) or to $T_{p2} \cong 780$ °C (ICCGHAZ). During cooling the chosen $\Delta t_{8/5}^{p2}$ or $\Delta t_{5/3}^{p2}$ were followed, where $\Delta t_{5/3}^{p2} = 2 \times \Delta t_{8/5}^{p2}$ if $T_0 = 50$ °C (Equation (4)). The metallographic appearance of the formed OCCGHAZ at $\Delta t_{8/5}^{p2} \cong 25$ s is almost the same as that in Figure 2., whereas the microstructure of the ICCGHAZ with $\Delta t_{5/3}^{p2} \cong 50$ s is as shown in Figure 4.

EXPERIMENTAL RESULTS

The austenite that forms during the heating phase of the thermal cycles decomposes during the cooling. The starting point for the simulation of the CGHAZ is the as-

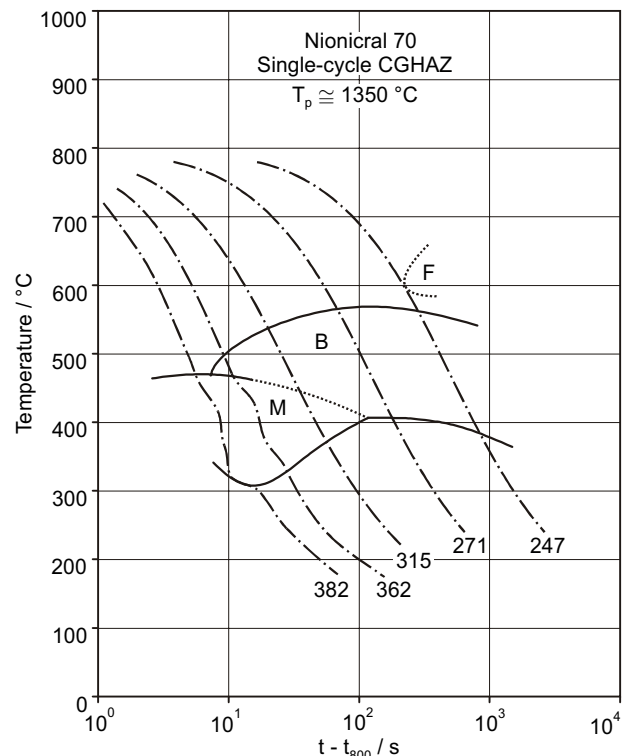


Figure 5. CCT diagram valid for the CGHAZ

Slika 5. CCT dijagram za važeći grubozrnati ZUT

delivered BM, whereas the starting point for the simulation of the OCCGHAZ and the ICCGHAZ is the CGHAZ.

Examples the start and finish of the austenite's decomposition to bainite (*Bs*, *Bf*) and martensite (*Ms*, *Mf*) during cooling from $T_{p1} \cong 1350\text{ }^\circ\text{C}$ and $T_{p2} \cong 780\text{ }^\circ\text{C}$ with $\Delta t_{8/5} \cong 9\text{ s}$ and $\Delta t_{5/3} \cong 18\text{ s}$ are indicated on the dilatometric curves in Figure 2. The analysis of such curves of the thermal cycles with the same T_p , but with different cooling rates, makes it possible to construct a CCT diagram that is valid for welding conditions:

1. The microstructure of the CGHAZ (Figure 5.) is formed if thermal cycles with $T_p \cong 1350\text{ }^\circ\text{C}$ are applied to the BM.
2. The microstructure of the OCCGHAZ (Figure 6.) is formed if thermal cycles with $T_p \cong 960\text{ }^\circ\text{C}$ are applied to the CGHAZ.

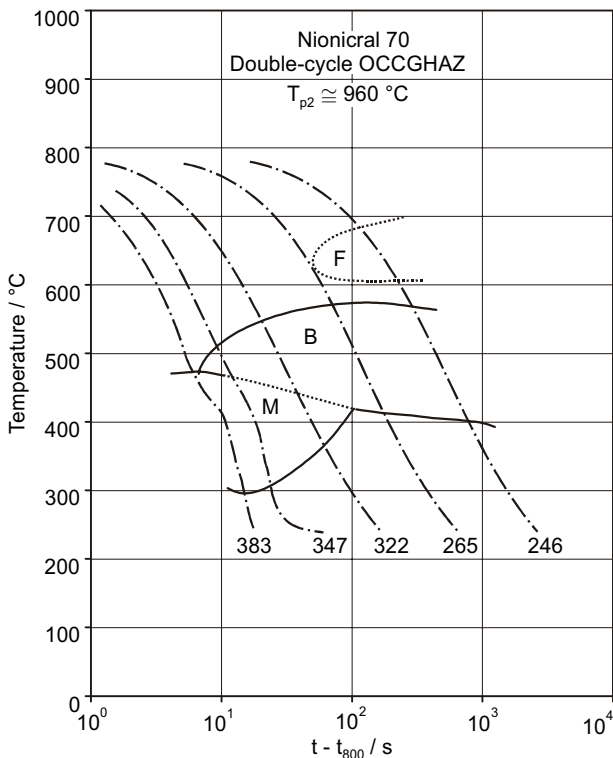


Figure 6. CCT diagram valid for the OCCGHAZ
Slika 6. CCT dijagram važeći za nadkritički zagrijan grubozrnatu ZUT

3. The microstructure of the ICCGHAZ (Figure 7.) is formed if thermal cycles with $T_p \cong 780\text{ }^\circ\text{C}$ are applied to the CGHAZ (because $Ac_1 < T_{p2} < Ac_3$ the diagram is valid for the transformed part).

Cooling curves with $\Delta t_{8/5} \cong 5, 9, 25, 100$ and 400 s and hardness, HV10, are shown in Figures 5. to 7.

When samples of the CGHAZ are simulated (Figure 5.) the starting microstructure consists of tempered martensite and bainite. When samples of the OCCGHAZ and ICCGHAZ are simulated (Figures 6. and 7.) the starting microstructure consists of either coarse-grained martensite

($\Delta t_{8/5} \leq 8$ to 9 s), martensite and bainite ($9 < \Delta t_{8/5} \cong 50\text{ s}$), pure bainite ($50 < \Delta t_{8/5} < 400\text{ s}$) or bainite with some ferrite ($\Delta t_{8/5} = 400\text{ s}$) (see Figure 5.).

The primary austenitic grain size of the CGHAZ varies from $120\text{ }\mu\text{m}$ ($\Delta t_{8/5} \cong 5\text{ s}$) to $250\text{ }\mu\text{m}$ ($\Delta t_{8/5} \cong 400\text{ s}$), whereas the grain size of the as-delivered BM was ASTM10 [6].

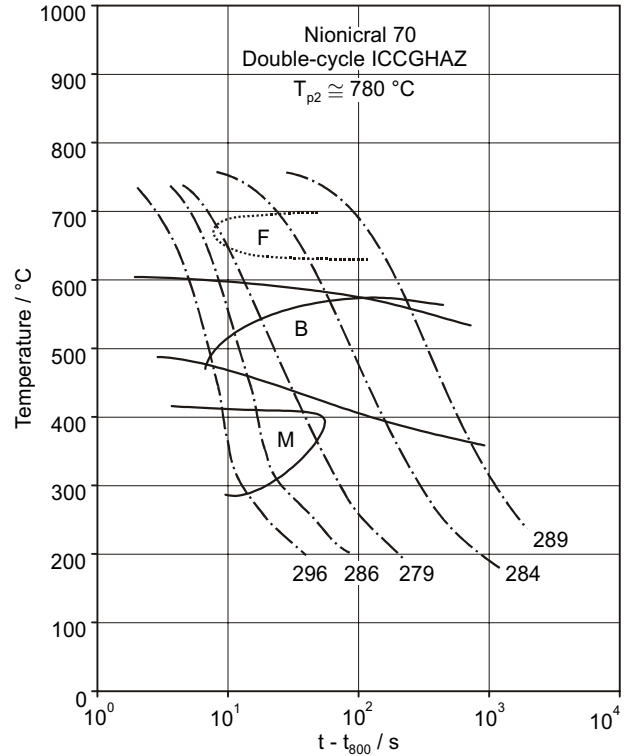


Figure 7. CCT diagram valid for the ICCGHAZ
Slika 7. CCT dijagram važeći za interkritički zagrijan grubozrnatu ZUT

The impact-toughness, CVN, at $-40\text{ }^\circ\text{C}$ and the HV10 of the single-cycle CGHAZ are shown in Figure 8. If the CGHAZ consists only of martensite (Figure 5.) the HV10

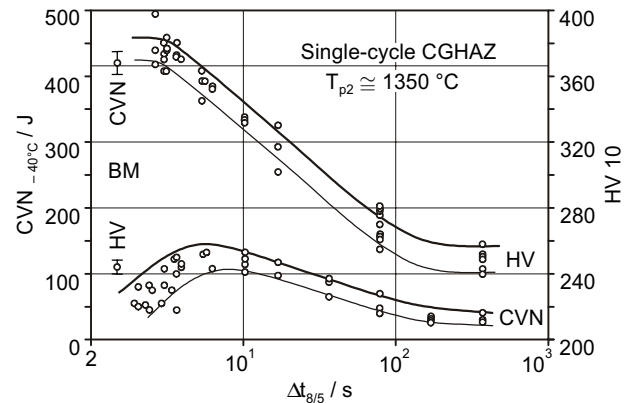


Figure 8. CVN and HV10 of the CGHAZ versus $\Delta t_{8/5}$
Slika 8. Žilavost i tvrdoća grubozrnatog ZUT obzirom na $\Delta t_{8/5}$

is constant. The CVN increases with the $\Delta t_{8/5}$ if pure martensite exists. If $\Delta t_{8/5} > 9$ s, the HV10 decreases linearly on a logarithmic scale until the appearance of the ferrite, whereas the CVN decreases.

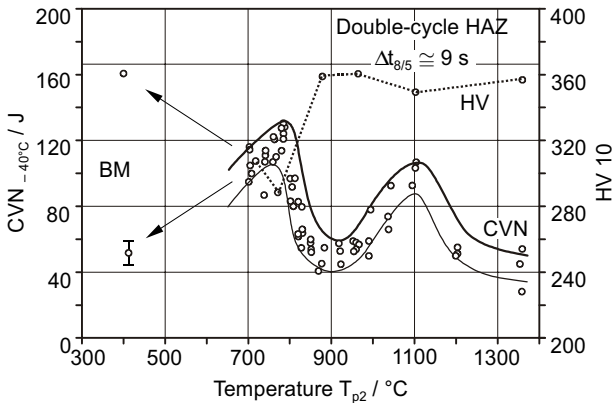


Figure 9. CVN and HV10 of the double-cycle HAZ at the FL versus T_{p2} if $\Delta t_{8/5} \approx 9$ s
 Slika 9. Žilavost i tvrdoća dvoprolaznog ZUT na crti taljenja obzirom na T_{p2} kad je $\Delta t_{8/5} \approx 9$ s

The CVN and HV10 of the double-cycle HAZ with $\Delta t_{8/5} \approx 9$ s ($\Delta t_{5/3} \approx 18$ s) and $\Delta t_{8/5} \approx 25$ s ($\Delta t_{5/3} \approx 50$ s)

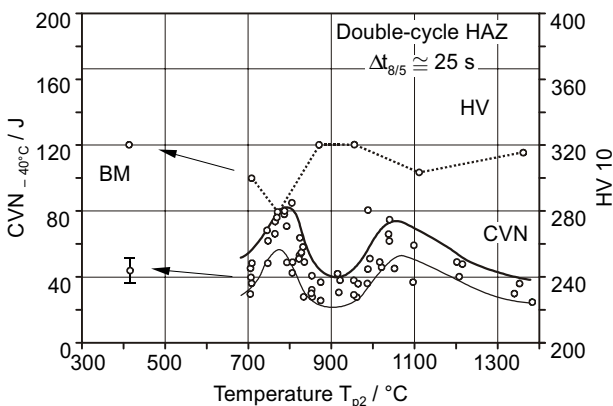


Figure 10. CVN and HV10 of the double-cycle HAZ at the FL versus T_{p2} if $\Delta t_{8/5} \approx 25$ s
 Slika 10. Žilavost i tvrdoća dvoprolaznog ZUT na crti taljenja obzirom na T_{p2} kad je $\Delta t_{8/5} \approx 25$ s

are shown in Figure 9. and 10. The properties are compared with those of the CGHAZs:

1. Despite reheating the CGHAZ only to Ac_1 the CVN is significantly improved. The improvement increases up to 780 °C, whereas the HV10 decreases.
2. When T_{p2} approaches 900 °C, i.e. the Ac_3 of the BM, the CVN decreases, whereas the HV10 increases.
3. When T_{p2} approaches 1150 °C the CVN increases; the HV10 is slightly changed.
4. At $T_{p2} > 1150$ °C the CVN decreases; the HV10 is not significantly changed.

DISCUSSION

The heating rate during the heating sequence of a thermal cycle using conventional welding techniques is in the range 200 to 300 K/s. The reverse martensitic transformation could, therefore, occur in the as-quenched martensite. This is not the case, however, if particles of cementite are precipitated after quenching. They are the result of either an intentional tempering (BM) or auto-tempering (HAZ). The latter is more likely to occur in steels with a higher M_s ($M_s = 470$ to 480 °C in Figure 5.).

According to the Fe-Fe₃C phase-diagram the reactions $\alpha + Fe_3C \rightarrow \gamma$ and $\alpha \rightarrow \gamma$ begin when Ac_1 and Ac_3 are exceeded. However, the cementite must be surrounded by ferrite for the former reaction to take place. The latter reaction acts along the G-O-S line when an appropriate carbon concentration is reached.

Due to rapid heating a substantial amount of superheating occurs before the transformation starts. The degree of superheating depends on the heating rate, which is a function of the heat input as well as the thermal properties and thickness of the BM. The dissolution of the cementite and the formation of the γ -phase as well as the diffusion of carbon into the ferrite are substantially delayed. In addition, when the γ -phase is formed as a result of both reactions the austenite is non-homogeneous. The concentration of the carbon in the vicinity of a dissolve Fe₃C particle is higher than it is further away. The carbon concentration in the just-formed γ -phase that is the result of the $\alpha \rightarrow \gamma$ reaction is lower than before, and some time is needed for homogenisation. The diffusion is faster in the case of higher superheating.

At a fixed temperature, the austenite at the FL is more heterogeneous if the heating rate is higher. When the applied thermal cycle reaches T_p the carbon-dissolution, the phase-transformation and the homogenisation are immediately slowed or even stopped.

Thus, the consequence of rapid heating in the first sequence of the thermal cycle is either a partially austenised previous microstructure or a fairly non-homogeneous austenite. The result of the decomposition of a non-homogeneous austenite is a more heterogeneous HAZ microstructure, as expected from the average chemical composition of the BM.

The size of the grains at the beginning of the decomposition is also important for the final microstructure. A high T_p during the thermal cycle at the FL is the reason for the grain growth. Precipitates hinder grain growth by pinning the grain boundaries if they are finely dispersed and still exist at the T_p . Less-stable precipitates are dissolved at the temperature where the grains can grow, whereas more stable precipitates are coarsened. Their dispersion is therefore lower and they are less effective in controlling the grain growth.

The bainite was found in the CGHAZ at $\Delta t_{8/5} = 7$ to 8 s. Some amount of bainite in a predominately martensitic microstructure increases the fracture resistance of the CGHAZ in HSLA structural steels. Ferrite was found in the CGHAZ only for $\Delta t_{8/5} = 400$ s. The most favourable sites for ferrite nucleation are the grain corners, the grain boundaries and the inclusions.

When two cycles were applied and $T_{p2} > A_{c3}$, bainite was found already at $\Delta t_{8/5} = 5$ s. Ferrite was observed at $\Delta t_{8/5} = 100$ s. The M_s was slightly lower than that in the CGHAZ; the HV10 of the pure martensite was the same (compare Figure 5. and 6.). The presence of ferrite does not lower the HV10 of the ferritic-bainitic-martensitic microstructure. The existence of harder micro-constituents in the predominantly bainitic-martensitic microstructure with a higher carbon-content prevails over the softer one transformed at a higher temperature (ferrite). The density of favourable sites for ferrite nucleation at the grain corners and boundaries is higher in fine-grained metals. However, ferrite is formed earlier in the developing coarse-grained microstructure of the OCCGHAZ than in the CGHAZ.

Only part of the previous CGHAZ microstructure was re-transformed during the application of the second thermal cycle to $T_{p2} = 780$ °C. Even during the fastest cooling a bainitic-martensitic microstructure was formed. The M_s was at least 50 K lower than that in the CGHAZ and ferrite was detected already at $\Delta t_{8/5} = 25$ s.

It has to be stressed that the HV10 in Figure 7. corresponds to the microstructure shown in Figure 4., not only to that represented by the CCT diagram in Figure 7. The ICCGHAZ actually consists of the microstructure from Figure 7. with a share of 60 to 70 % (such a percentage of the CGHAZ was retransformed at $T_{p2} \cong 780$ °C). The rest is the tempered microstructure from Figure 3. The first part has a slightly higher carbon content. This could be the main reason for the improved CVN at $T_p < A_{c3}$ in Figure 6. and 7.

CONCLUSIONS

A certain amount of heat needs to be put into the BM in order to fuse a part of it and create a weld-joint. This heating, however, affects the microstructure. A CGHAZ, a OCCGHAZ or a ICCGHAZ exists at the FL after welding. A welding simulation is a suitable method for preparing samples of different HAZ sub-zones. Afterwards, the microstructure and the properties of these sub-zones can be predicted.

The properties of the HAZ depend on the overall thermal regime of the welding. The austenitic grain size is the result of the thermal cycle with the highest T_p . This is the result of the first weld pass, which actually defines the position of the FL. The last thermal cycle, which changes the microstructure, whether completely or partially, i.e. its T_p and $\Delta t_{8/5}$ ($\Delta t_{5/3}$), is decisive for determining the final micro-constituents. The more-or-less non-homogenised austenite at the beginning of the cooling is the main reason why the microstructure and the properties of the HAZ are not easy to forecast.

REFERENCES

- [1] K. Easterling, Introduction to the Physical Metallurgy of Welding, Butterworths, London 1983, pp. 104-156.
- [2] L. Karlsson, Thermal Stresses in Welding, Thermal Stresses I, Edited by R. B. Hetnarski, Elsevier Science Publisher, 1986.
- [3] SMITWELD, Thermal Cycle Simulator, Instruction manual.
- [4] T. Haze, Y. Ohno, Y. Kawashima, R. Chijiiva, S. Aihara, K. Uchino, Y. Tomita, H. Mimura, Steel Plates with Superior HAZ Toughness for Offshore Structures, Nippon Steel Technical Report, 36, 39 - 48, 1988.
- [5] R. D'Haeyer and J. Defourny, Annual Assembly of the International Institute of Welding 1990, IIW Doc.: IX-1606 - 90.
- [6] V. Gliha, Analiza nosilnosti homogenih večvarkovnih zvarnih spojev pri utrujanju z ozirom na vplive parametrov varjenja in gradnje vara, Doktorska disertacija, Univerza v Ljubljani, Naravoslovno-tehniška Fakulteta, 1998, Ljubljana.